NASA/TM-2006-214505

Quasi-Static 3-Point Reinforced Carbon-Carbon Bend Test and Analysis for Shuttle Orbiter Wing Leading Edge Impact Damage Thresholds

Edwin L. Fasanella
Langley Research Center, Hampton, Virginia

Sotiris Kellas
General Dynamics, Advanced Information Systems, Hampton, Virginia

September 2006

The NASA STI Program Office . . . in Profile

Since its founding, NASA has been dedicated to the advancement of aeronautics and space science. The NASA Scientific and Technical Information (STI) Program Office plays a key part in helping NASA maintain this important role.

The NASA STI Program Office is operated by Langley Research Center, the lead center for NASA's scientific and technical information. The NASA STI Program Office provides access to the NASA STI Database, the largest collection of aeronautical and space science STI in the world. The Program Office is also NASA's institutional mechanism for disseminating the results of its research and development activities. These results are published by NASA in the NASA STI Report Series, which includes the following report types:

- TECHNICAL PUBLICATION. Reports of completed research or a major significant phase of research that present the results of NASA programs and include extensive data or theoretical analysis. Includes compilations of significant scientific and technical data and information deemed to be of continuing reference value. NASA counterpart of peer-reviewed formal professional papers, but having less stringent limitations on manuscript length and extent of graphic presentations.

- TECHNICAL MEMORANDUM. Scientific and technical findings that are preliminary or of specialized interest, e.g., quick release reports, working papers, and bibliographies that contain minimal annotation. Does not contain extensive analysis.

- CONTRACTOR REPORT. Scientific and technical findings by NASA-sponsored contractors and grantees.

- CONFERENCE PUBLICATION. Collected papers from scientific and technical conferences, symposia, seminars, or other meetings sponsored or co-sponsored by NASA.

- SPECIAL PUBLICATION. Scientific, technical, or historical information from NASA programs, projects, and missions, often concerned with subjects having substantial public interest.

- TECHNICAL TRANSLATION. English-language translations of foreign scientific and technical material pertinent to NASA's mission.

Specialized services that complement the STI Program Office's diverse offerings include creating custom thesauri, building customized databases, organizing and publishing research results ... even providing videos.

For more information about the NASA STI Program Office, see the following:

- Access the NASA STI Program Home Page at ***http://www.sti.nasa.gov***

- E-mail your question via the Internet to help@sti.nasa.gov

- Fax your question to the NASA STI Help Desk at (301) 621-0134

- Phone the NASA STI Help Desk at (301) 621-0390

- Write to:
  NASA STI Help Desk
  NASA Center for AeroSpace Information
  7121 Standard Drive
  Hanover, MD 21076-1320

NASA/TM-2006-214505

Quasi-Static 3-Point Reinforced Carbon-Carbon Bend Test and Analysis for Shuttle Orbiter Wing Leading Edge Impact Damage Thresholds

Edwin L. Fasanella
Langley Research Center, Hampton, Virginia

Sotiris Kellas
General Dynamics, Advanced Information Systems, Hampton, Virginia

National Aeronautics and
Space Administration

Langley Research Center
Hampton, Virginia 23681-2199

September 2006

Available from:

NASA Center for AeroSpace Information (CASI)
7121 Standard Drive
Hanover, MD 21076-1320
(301) 621-0390

National Technical Information Service (NTIS)
5285 Port Royal Road
Springfield, VA 22161-2171
(703) 605-6000

Quasi-Static 3-Point Reinforced Carbon-Carbon Bend Test and Analysis for Shuttle Orbiter Wing Leading Edge Impact Damage Thresholds

Edwin L. Fasanella, NASA Langley Research Center
Sotiris Kellas, General Dynamics

Abstract

Static 3-point bend tests of Reinforced Carbon-Carbon (RCC) were conducted to failure to provide data for additional validation of an LS-DYNA RCC model suitable for predicting the threshold of impact damage to shuttle orbiter wing leading-edge panels. LS-DYNA predictions correlated well with the average RCC failure load, and showed good agreement in matching the load versus deflection response. However, correlating the detectable damage using nondestructive evaluation (NDE) methods with the cumulative damage parameter in LS-DYNA material model Mat58 was not readily achievable. The difficulty of finding internal RCC damage with NDE and the high sensitivity of the Mat58 damage parameter to the load near failure made the task very challenging. In addition, damage mechanisms for RCC due to dynamic impact of debris such as foam and ice are not equivalent to damage mechanisms due to a static loading.

Background

The criterion defining impact damage threshold of the wing leading edge panels used by the Orbiter Project was changed from a through crack to internally detectable nondestructive evaluation (NDE) damage plus some outer silicon carbide (SiC) coating loss. This change presented a challenge to the existing shell model of shuttle orbiter Reinforced Carbon-Carbon (RCC) since delamination and coating loss cannot be directly represented in a shell element. Consequently, simple static 3-point RCC bend tests were proposed by the NASA Engineering and Safety Center (NESC) as a useful test in addition to ballistic testing to assist in calibrating the LS-DYNA RCC material model for predicting internal RCC damage caused by debris impacts. The tests could also serve as a "level 1" validation test for RCC material. Since the test was quasi-static, loads and displacements could be accurately measured experimentally. However, static and dynamic damage and failure mechanisms are often very different. Static tests allow the entire structure to move without inertial loading effects. Thus, the forces are more global and the internal stresses more distributed. Dynamic loads are rapidly applied and produce shock effects with complex stress waves. Inertial effects become extremely important. Also, strain-rate effects must be considered, and the dynamic stresses are both much higher and localized near the area of contact.

RCC 3-point Bend Test Setup

Southern Research Institute (SRI) cut twenty 3-point flex coupons, a compression test coupon, a tension test coupon, and a scrap for testing coating crush strength from RCC test panel TC3-11. Static and quasi-static 3-point bend tests of 19-ply RCC coupons 1.0-in. wide x 5.8-in. long (5.25-in. gage length) were conducted with incremental loading and NDE after each load cycle to validate the LS-DYNA RCC threshold of damage predictions. The objectives of the tests were to: 1) study the damage initiation and propagation in the RCC samples under quasi-static 3-point bend loading, 2) determine the

NDE detectable damage threshold, 3) correlate first detectable NDE damage with LS-DYNA damage parameter(s), and 4) determine if delamination can be initiated in static RCC bend tests, and if so, can that delamination be correlated with LS-DYNA damage parameters. A picture of the 3-point bend test set-up is shown in Figure 1.

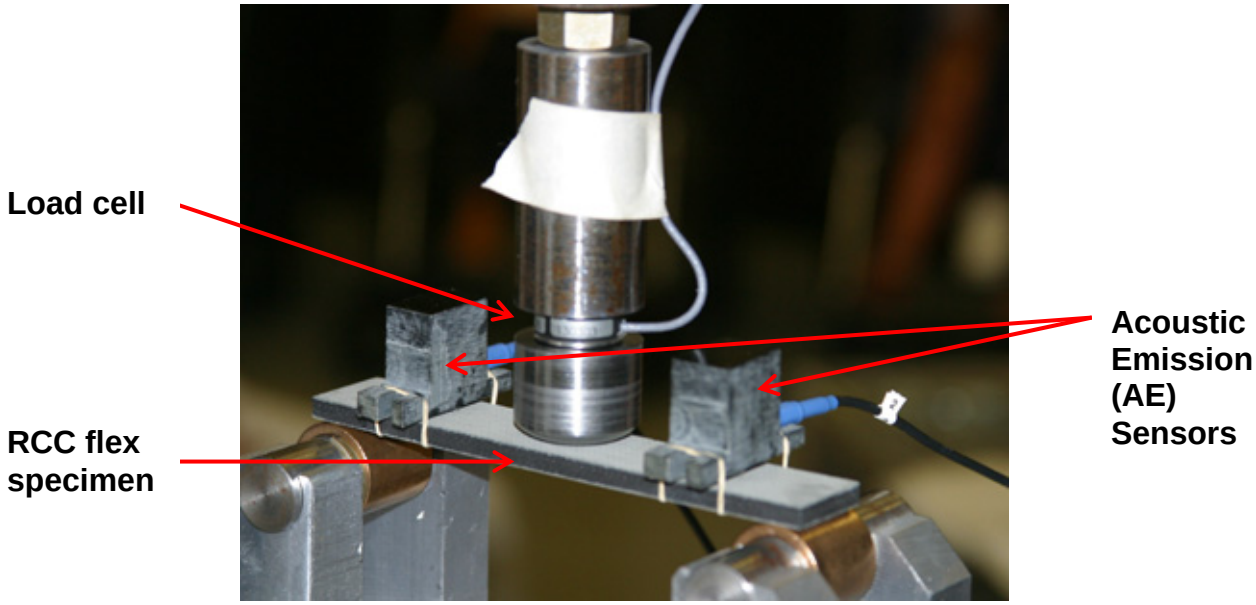

Figure 1. Level 1 three-point bend test of RCC coupon

Experimental Test Description

The first 13 of the 20 samples were tested at low loading rates. For all tests, acoustic emission (AE) was used to monitor damage development. Unless otherwise noted, the displacement rate used for each test was 0.1 inches-per-minute (ipm). A brief summary of loading and NDE applied to each sample is as follows:

Sample flex-1. Sample 1 was first loaded to 70 lbs. and then unloaded. A permanent set at the center for the first loading and loading cycle to 70 lbs. was measured to be 0.015 inches (Figure 2). The sample was then reloaded to 80, 90, 100, 110, 120, and 130 lb. (See figures 2 – 4). The magnitude of permanent set becomes less and less with each loading cycle. After each loading cycle, the sample was evaluated with three NDE techniques (radiography, thermography and Eddy current). The final loading cycle at 130 pounds did not result in failure of the specimen. From the loading curves shown in Figure 2, it is noted that the slope increases for subsequent loadings after the first load cycle similar to work hardening in metals. The increase in stiffness is postulated to be due to fiber straightening. The permanent set is readily visible as a bowing of the specimen. For the final few loadings, the slope returns back to that of the original curve (Figure 3).

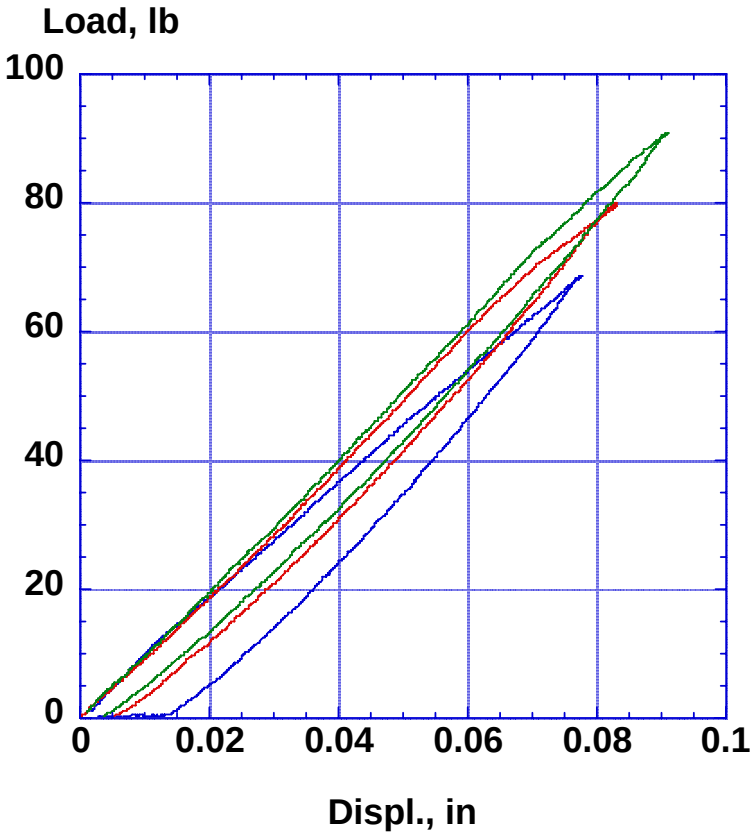

Figure 2. First three loading cycles to 70 (blue), 80 (red), and 90 lbs (green) for specimen flex-1. Note that the slope of the loading curves increases for the second and third loading cycles for loads above 20 pounds. Also, note the hysteresis in the first loading cycle versus the second and third cycles.

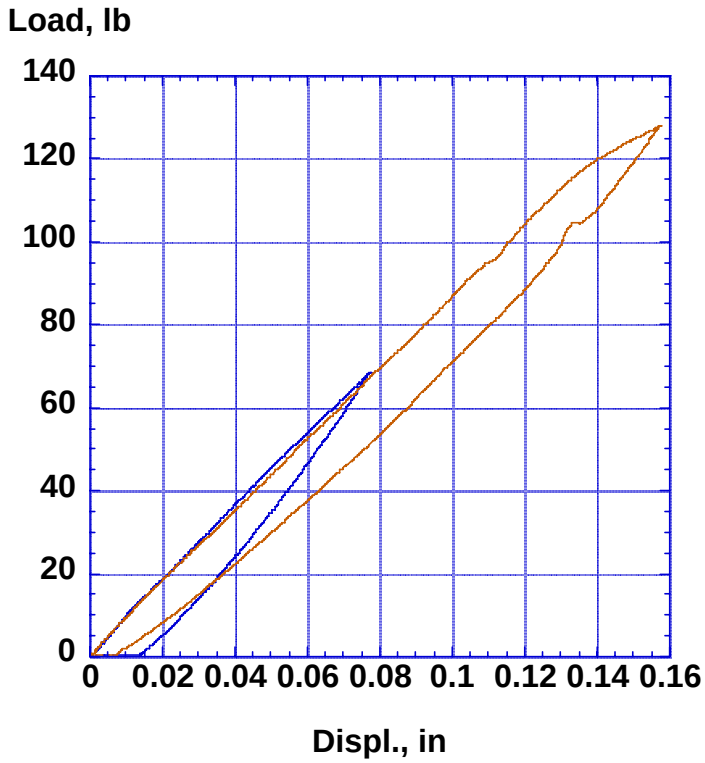

Figure 3. First (70 lbs) and last (130 lbs) loading cycles for specimen flex-1. Note the slope of the 130 pound curve is now below the initial curve for loads above 20 pounds.

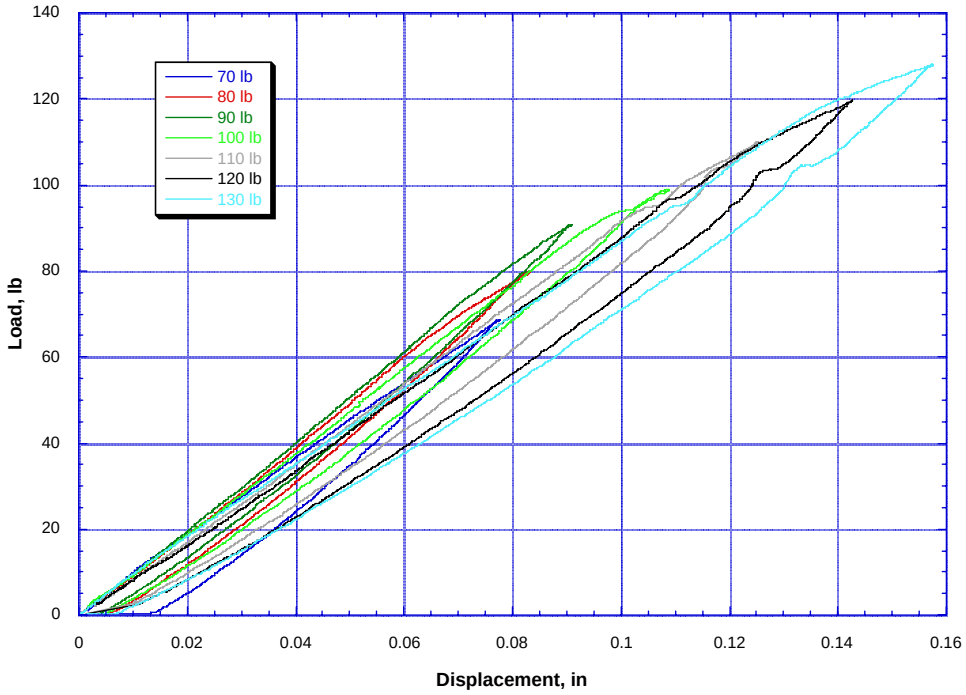

Figure 4. Combined curves for all loading cycles for specimen flex-1.

Sample flex-2. This specimen was tested to ***failure*** (132 lb.) while damage initiation was monitored with a close up video and digital camera. Close-up stills of the bottom surface were taken during sample loading with a digital camera every 3 seconds.

Sample flex-3. This specimen was tested to ***failure*** (132 lb.) while damage initiation was monitored with a close up video and digital camera. Close-up stills of the bottom surface were taken during sample loading with a digital camera every 3 seconds.

Sample flex-4. This specimen was loaded sequentially at two increasing load levels, 103 lb and 126 lb. The displacement rate for this sample was 1.0 ipm. After each load cycle the sample underwent three NDE techniques (radiography, thermography and Eddy current).

Sample flex-5. This specimen was loaded sequentially at two increasing load levels, 120 and 130 lb. After each load cycle the sample underwent three NDE techniques (radiography, thermography and Eddy current). After the conventional NDE tests, this sample was also sent for micro-CT scans slices at 100 and 200 microns.

Sample flex-6. This specimen was tested to ***failure*** (123 lb.) while damage initiation was monitored with a close up video and digital camera. Close-up stills of the bottom surface were taken during sample loading with a digital camera every 3 seconds.

Sample flex-7. This specimen was tested to ***failure*** (126 lb.) while damage initiation was monitored with a close up video and digital camera. Close-up stills of the bottom surface were taken during sample loading with a digital camera every 3 seconds.

Sample flex-8. This specimen was tested in one loading to ***failure***, which occurred at 127 pounds. The load versus center displacement curve for this sample is depicted in Figure 5. The plot is labeled to reflect AE activity and load levels where critical events occur such as cracking of the SiC coating, etc.

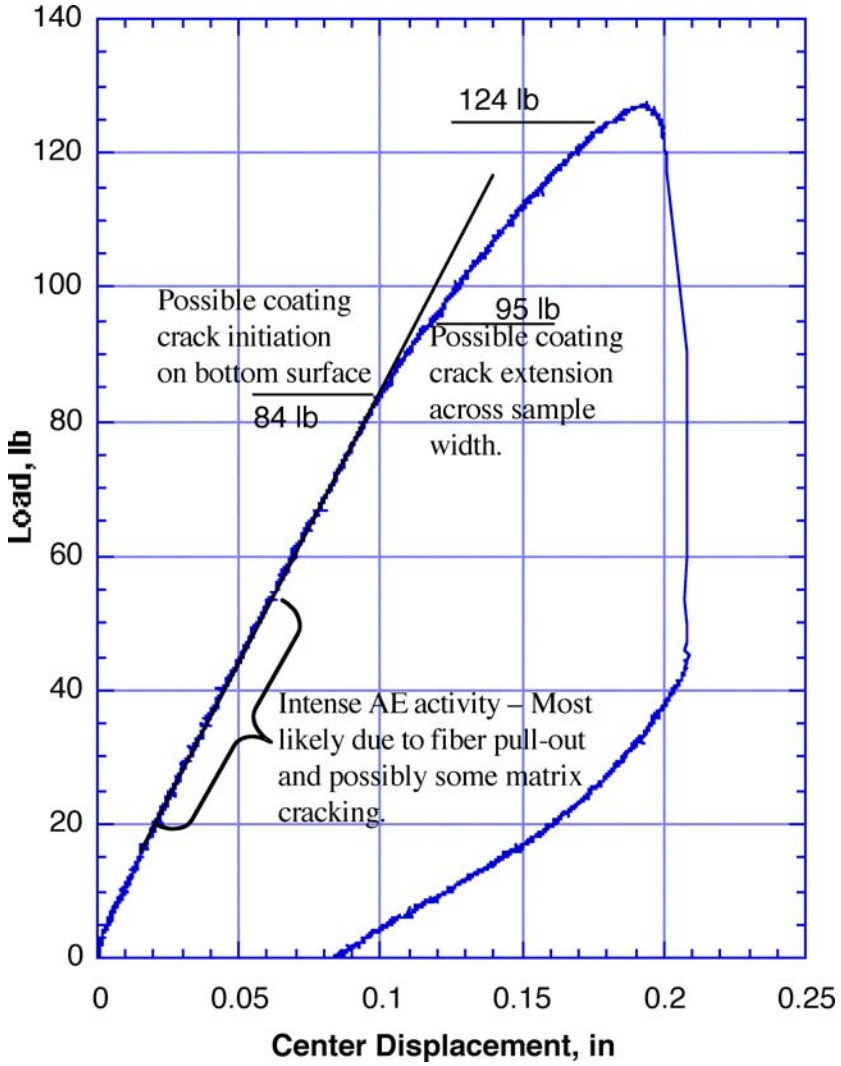

Figure 5. Load vs. displacement for specimen flex-8.

Sample flex-9. This specimen was tested to 100 lb while damage initiation was monitored with a close up video and digital camera as illustrated in Figures 6 and 7. Close-up stills of the bottom surface were taken during sample loading with a digital camera every 3 seconds. It has been verified using digital photography that detrimental damage first occurs on the bottom surface in the form of tensile coating cracks. For sample flex-9 this behavior was verified at ~85 lb. but could possibly be initiating as low as 69 lb., where the load/displacement curve deviates from linearity. NDE could not detect these surface cracks definitively.

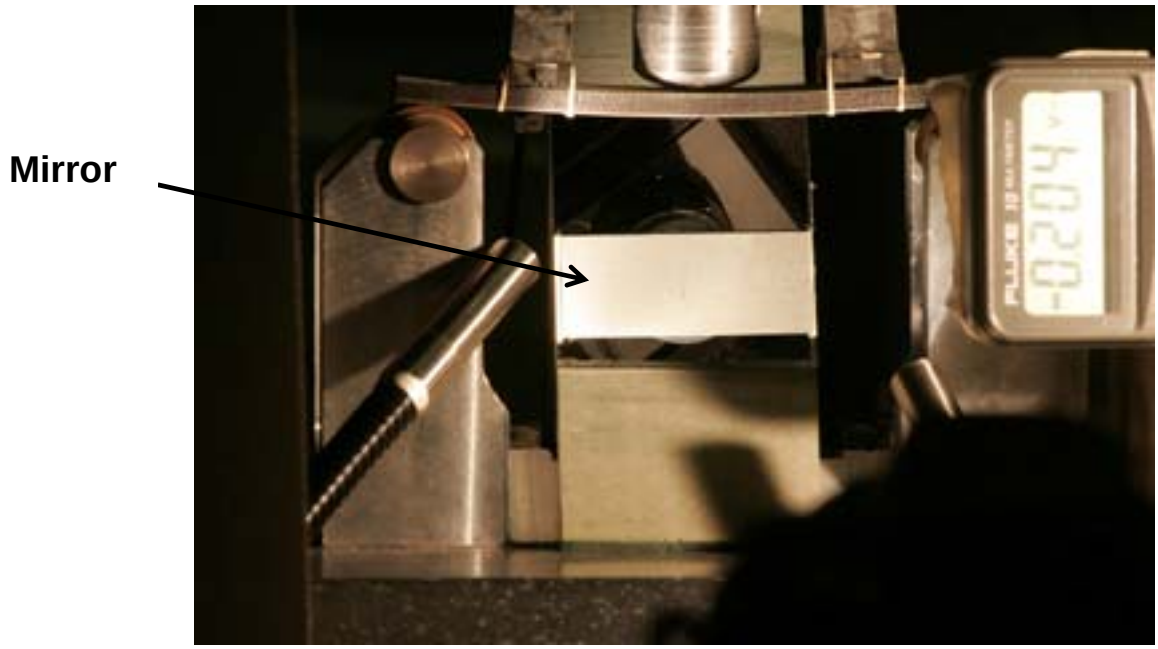

Figure 6. 3-Point bend test with mirror to view the crack growth in the lower layer of SiC with a digital camera.

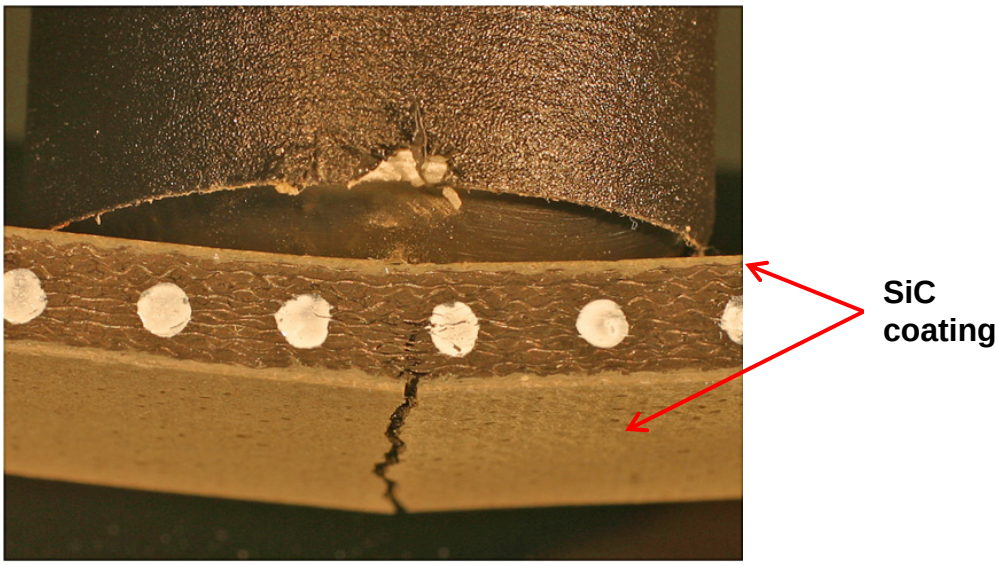

Figure 7. Typical failure of bend specimen. Dots were used for photogrammetry.

Sample flex-12. This specimen was tested to 100 lb while damage initiation was monitored with a close up video and digital camera. Close-up stills of the bottom surface were taken during sample loading with a digital camera every 3 seconds. After loading, the sample underwent two NDE techniques (thermography and Eddy current). The sample was then reloaded to a maximum load of 100 lb for 5 cycles while damage was monitored and recorded optically.

Sample flex-13. This specimen was tested to 100 lb while damage initiation was monitored with a close up video and digital camera. Close-up stills of the bottom surface

were taken during sample loading with a digital camera every 3 seconds. After loading, the sample underwent two NDE techniques (thermography and Eddy current). Subsequently, the sample was reloaded to a maximum load of 100 lb for 5 cycles while damage was monitored and recorded optically.

Sample flex-16. This specimen was tested to 110 lb while damage initiation was monitored with a close up video and digital camera. Close-up stills of the bottom surface were taken during sample loading with a digital camera every 3 seconds. After loading, the sample underwent two NDE techniques (thermography and Eddy current). The sample was reloaded to a maximum load of 110 lb for 5 cycles while damage was monitored and recorded optically.

Sample flex-17. This specimen was tested to 110 lb while damage initiation was monitored with a close up video and digital camera. Close-up stills of the bottom surface were taken during sample loading with a digital camera every 3 seconds. After loading, the sample underwent two NDE techniques (thermography and Eddy current). The sample was reloaded to a maximum load of 110 lb for 5 cycles while damage was monitored and recorded optically.

3-point Bend Tests at Increased Quasi-Static Loading Rate

The next six tests were accomplished at a loading rate of 20 ipm to determine if rate effects could be detected for relatively low velocities.

Sample flex-10 was loaded to ***failure*** at 20 ipm. Failure occurred at 126 lbs.
Sample flex-11 was loaded to ***failure*** at 20 ipm. Failure occurred at 131 lbs.
Sample flex-14 was loaded at a loading rate of 20 ipm from zero to 105 lbs six times.
Sample flex-15 was loaded at a loading rate of 20 ipm from zero to 100 lbs six times.
Sample flex-18 was loaded at a loading rate of 20 ipm from zero to 100 lbs five times.
Sample flex-20 was loaded to **failure** at 20 ipm. Failure occurred at 132 lbs.

Ultrasonic NDE testing

The following specimens were shipped to NASA Glenn Research Center (GRC) to be evaluated using ultrasonic C-scan through transmission. The results for specimens 13, 12, 9, and 1 are shown in Figure 8. Specimen 1 is the specimen at the bottom of the figure. There is a region at the center of specimen 1 that is slightly darker than for the other specimens. This dark band may indicate some damage accumulation, but is open to question. The average breaking load of all failed specimens was 128.6 lb with a standard deviation of 3.2 lbs. Thus, specimen flex-1 would be expected to have damage accumulation near the center as it was loaded multiple times. The last loading cycle was up to a maximum load of 130 lbs.

Sample flex-1 was loaded at 0.1 ipm in 10-lb increments from 70-130 lb.
Sample flex-4 was loaded at 1.0 ipm to 103 and then 126 lb.
Sample flex-5 was loaded at 0.1 ipm to 120 and then 130 lb.
Sample flex-9 was loaded at 0.1 ipm to 100 lb.
Sample flex-12 was loaded at 0.1 ipm 5 times to 100 lb.
Sample flex-13 was loaded at 0.1 ipm 5 times to 100 lb.
Sample flex-14 was loaded at 20 ipm 6 times to ~105 lb.
Sample flex-15 was loaded at 20 ipm 6 times to ~100 lb.
Sample flex-16 was loaded at 0.1 ipm 6 times to 110 lb.
Sample flex-17 was loaded at 0.1 ipm 6 times to 110 lb.
Sample flex-18 was loaded at 20 ipm 5 times to ~100 lb.

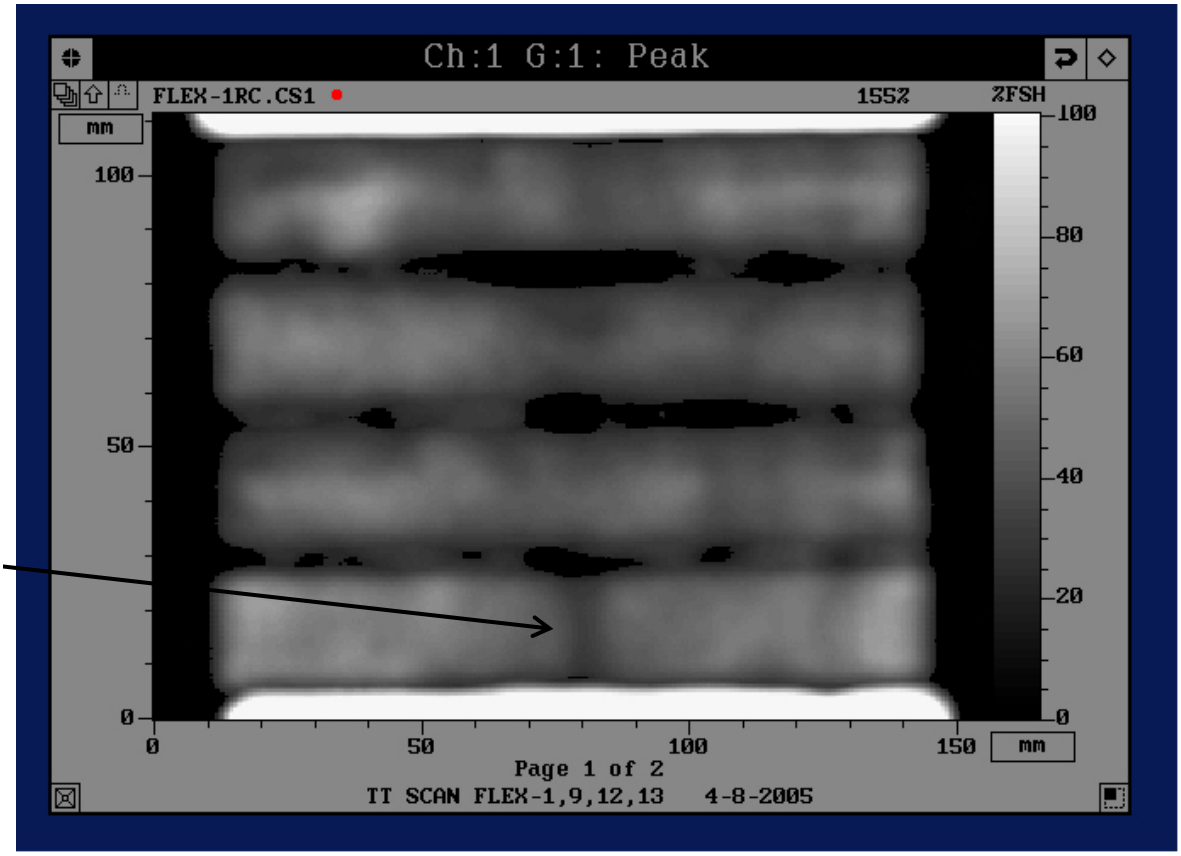

Figure 8. Ultrasonic C-scan transmission NDE results for specimens (from top down) 13, 12, 9 and 1. The arrow points to the dark band at the center of specimen 1.

Microfocus x-ray CT Scans of flex-5

NASA Langley has a "one-of-a-kind" computed tomography (CT) x-ray machine in conjunction with a mechanical loads machine as depicted in Figure 9. The equipment includes a 160 kev microfocus x-ray, a 56,000-lb. mechanical load machine, an optimal resolution of 12.5 microns, and a maximum field of 3.5-in, and an array of 8192 scintillation detectors.

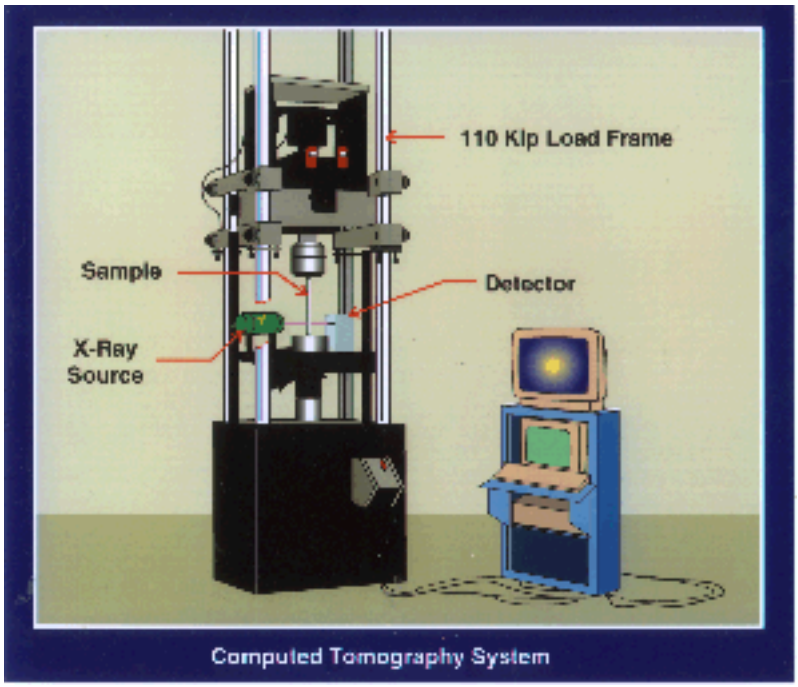

Figure 9. LaRC Computed Tomography System.

Specimen flex-5 was chosen for study using the LaRC microfocus CT-scan equipment. No load was applied. The scans were taken width-wise and are thus 1.0-in. x 0.233-in. in area. Note that "flex-5" was loaded at a load-rate of 0.1 ipm to 120 pounds and then at the same rate to 130 pounds. When examined post loading, no NDE-detectable damage was found using the suite of conventional NDE techniques (radiography, eddy-current, flash thermography). The first set of scanned "slices" for the region of maximum stress (near the center of specimen flex-5) was at 200 microns width. A second set of 100 micron (0.001 mm) slices were then made. Although multiple voids and micro-cracks could be detected, no definitive damage due to the repeated loading could be detected. No long cracks or delaminations or other NDE-detectable damage were found. Images from the second set of scans performed at 100 microns are shown in Figures 10 and 11. Again, voids and micro-cracks can be seen in the substrate as well as a clear view of the SiC coating and its micro-cracks, but no load-induced damage could be seen. Since no pre-test micro-CT scans were performed, micro-CT scans were performed at the ends of the specimen that were expected to be areas of low stress and hence no damage. The scans at the ends, seen in Figure 12 and 13, resembled the scans in the center. That is, there were randomly scattered voids and micro-cracks. Using the micro-CT scans, no conclusions could be reached as to damage of the center region due to loading. A summary of all test results is given in Table I.

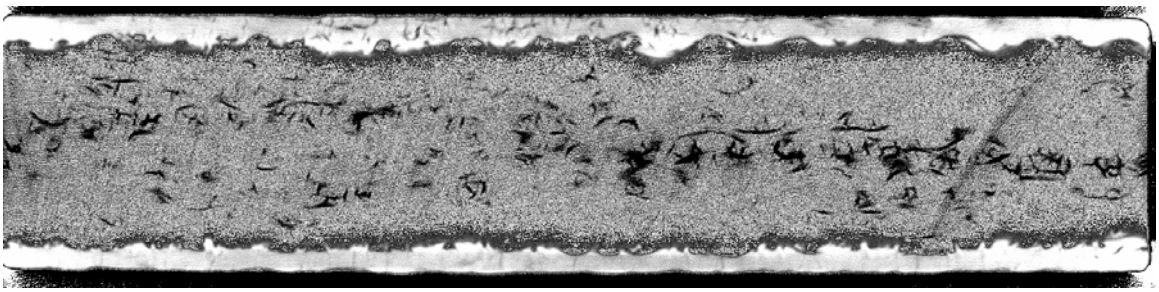

Figure 10. 100 micron scan of 1-in. x 0.233-in cross-section flex-5 near center of specimen where loading was maximum for the 3-point bend test.

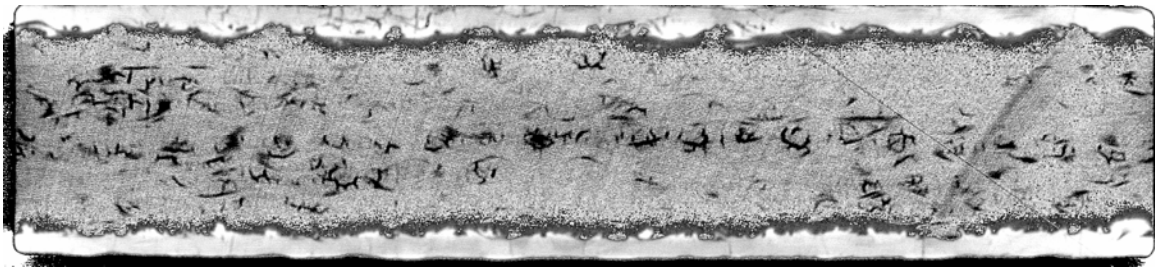

Figure 11. Next sequential 100 micron slice of flex-5 near center of specimen.

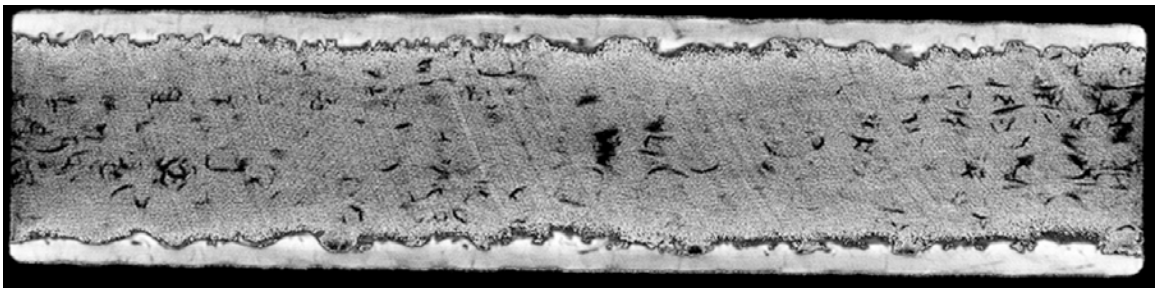

Figure 12. 100-micron scan taken at end of specimen where loading was very low.

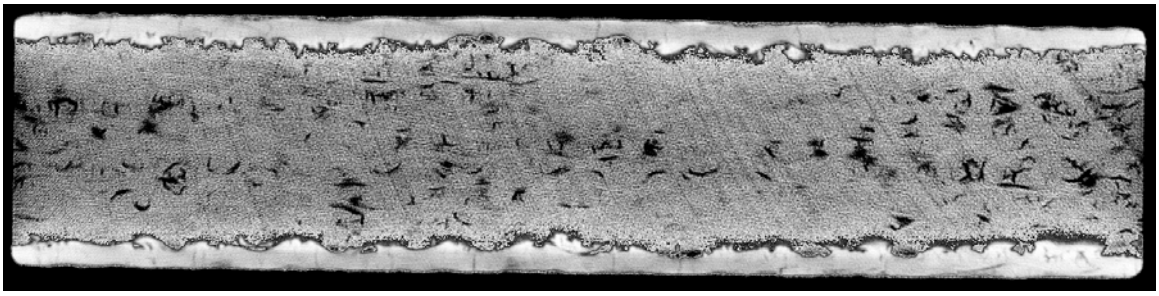

Figure 13. Next sequential 100-micron scan at end of specimen.

Table I. Summary of Static 3-point bend test results

Specimen	**Loading Rate ipm**	**NDE**	**Loading cycles**	**Max Load** lbs	**Complete Failure?**
Flex-1	0.1	x-ray, therm, eddy,ult.	7	130	No
Flex-2	0.1	Video, camera	1	132	Yes
Flex-3	0.1	Video, camera	1	132	Yes
Flex-4	0.1	x-ray, therm, eddy,ult.	2	126	No
Flex-5	0.1	Micro CT-scan, ult	2	130	No
Flex-6	0.1	Video, camera	1	123	Yes
Flex-7	0.1	Video, camera	1	126	Yes
Flex-8	0.1	None, one loading	1	127	Yes
Flex-9	0.1	picture every 3 sec, ult.	1	100	No
Flex-10	20		1	126	Yes
Flex-11	20		1	131	Yes
Flex-12	0.1	Camera, therm, eddy, ult	6	100	No
Flex-13	0.1	Video, camera, ult.	6	100	No
Flex-14	20	ultrasonics	6	105	No
Flex-15	20	ultrasonics	6	100	No
Flex-16		Video, cam, therm, eddy, ultrasonics	6	110	No
Flex-17	0.1	ultrasonics	6	110	No
Flex-18	20	ultrasonics	5	100	No
Flex-19	Not used				
Flex-20	20		1	132	Yes
		AVERAGE FAILURE Load		**128.6**	

Short Beam Shear Test

Since no NDE detectable delamination could be initiated and/or verified during these static 3-point bend tests, the NESC requested a series of short beam shear tests in another attempt to produce internal RCC damage/delamination. Several short-beam shear tests were performed with small RCC specimens with a one-inch span with similar results to the larger 3-point bend tests. The load was applied very slowly using displacement control, and surface displacements were monitored with video cameras and with photogrammetry. The first failure was always the tension failure at the bottom of the specimen. After several tests with no delaminations, a very small delamination occurred late in the loading sequence as shown in Figure 14. However, since the delamination was not the first failure, this mechanism could not be readily modeled and compared with analysis.

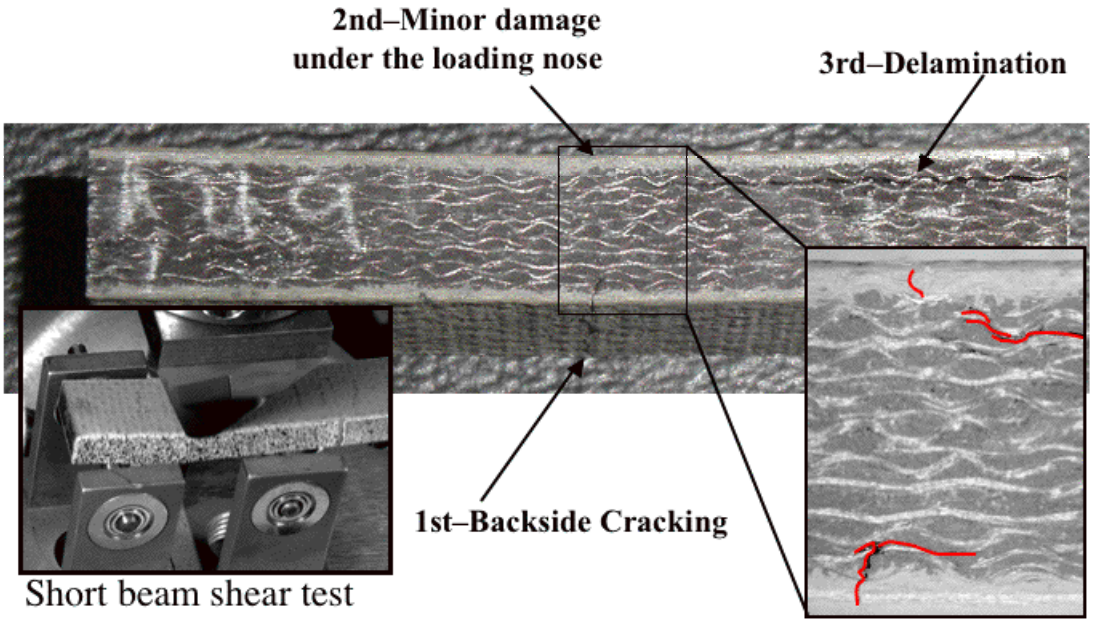

Figure 14. Short-beam shear test. The third failure late in the loading sequence is an apparent delamination.

Discussion of Test Results

As it turned out, the static 3-point bend test was not a good test method to produce internal NDE detectable damage comparable to dynamic induced internal damage. However, since the test was quasi-static, loads and displacements could be accurately measured experimentally and good comparisons with analysis up to and including breaking of the RCC were possible. Thus, the information proved very useful for additional level 1 validation of the LS-DYNA RCC model

The average failure load for all flex specimens (total of 8) loaded to failure (specimen breaks) was **128.6** pounds with a standard deviation of **3.2** pounds. Although AE recorded multiple events in every test, the other NDE techniques were not sensitive enough to resolve damage known to exist (and seen by digital camera) in loaded samples that were above the average failure load. The lowest load level after which NDE identifiable damage (using Eddy current) could be documented when scanned from the damaged side was 100 lb, while coating cracking had been documented optically to occur at as low as 50 lb. Moreover, gage-section AE events were recorded for applied loads as low as 10 lb. Damage accumulation was also verified through the observed hysterisis in the load versus displacement response.

Reloading of samples to the same maximum load produced very few subsequent AE events. The number of AE events also reduced as the number of load cycles increased. This finding leads to two important conclusions; (a) AE events NOT associated with damage propagation are insignificant, and (b) RCC samples have an inherent toughness (crack arresting, or damage tolerance capability) which prevents previously initiated

damage from propagating. Another, observation that supports point (b) is reduced hysteresis in load versus displacement response after two to three load cycles to the same maximum load.

Following two to three load cycles to the same maximum load, the slope of the load/displacement curve increases. During subsequent load cycles, load/displacement responses appear to revert back to the original response. One possible explanation for such behavior is two (or more) competing modes, such as, for example, detrimental matrix cracking and a beneficial mechanism such as fiber debonding (pull-out) that leads to fiber straightening.

Comparison of NDE damage between virgin, first load cycle, and subsequent 5 load cycles (to 110 lb) in samples flex-16 and flex-17 indicated a slight increase in damage accumulation. The same comparison for samples flex-12 and flex-13 showed a slight damage accumulation increase for only one of the two samples. This finding indicates that the 100 lb level is close to the average load at which samples could be loaded continuously without some degradation in material properties. The average gage section for samples 12 and 13 was 0.223-inch.

Photo-visual examination of crack initiation and propagation in samples flex-12, 13, 16, and 17 showed no new crack development after an additional 5 cycles, which is in agreement with the AE observations. Moreover, photography verified that cracks are not visible when samples are unloaded. This evidence helps explains why NDE techniques such as radiography and Eddy current cannot verify this type of damage. One important outcome from this study may be a new NDE procedure to improve NDE sensitivity. Since the study showed no damage propagation when samples are reloaded below a given maximum load, it might be possible to NDE samples (or panels) under a slight load, which will allow opening of the cracks and hence make them more visible to the NDE techniques. Or, if precision scanning of panel geometry could be made before and after missions, the detection of the minute permanent set due to an impact could be detectable.

Of all the currently used NDE techniques, AE proved to be the most sensitive. However, no damage mode could be associated with the AE signals. Photo-visual techniques, though cumbersome to use, proved to be extremely useful in monitoring crack initiation and propagation on the bottom SiC coating. Eddy current proved to be the most sensitive and hence useful technique when compared to radiography and thermography. The C-scan ultrasonic technique was also unable to unequivocally find areas of damage, although the center of specimen 1 did appear somewhat darker than the other specimens. Finally, micro-CT x-ray scans (100 micron slices) of flex-5 were unable to discern any crack growth, delaminations, or other internal damage.

Model Description- 3 Point Bend Test

Southern Research Institute (SRI) performed material testing on the tension and compression test coupons that were part of the panel that the flex coupons were cut from. SRI provided the complete stress-strain curves to failure that were used as input into LS-DYNA's Mat 58 material model. For all RCC models, Mat58 (MAT LAMINATED

COMPOSITE FABRIC) with failure was used as the material model for the RCC. The RCC material parameters required for LS-DYNA's Mat58 formulation are based on available RCC material data obtained by coupon testing to failure of laminates of varying thickness in tension and compression. There is a wide variation in the RCC material properties for as-fabricated material. A continuum damage model [1] is used in Mat58 to simulate internal damage with increasing load, which weakens the material and produces the nonlinear stress-strain curves. The damage parameter starts out at zero and approaches one at failure. By adjusting the strength and maximum strain values plus post maximum-strength parameters "SLIMC" and "SLIMT," the experimental stress-strain curves can be matched to a reasonable degree. Although RCC stress-strain curves have different moduli in tension and compression, the modulus in compression was used in Mat58. The RCC was modeled as 19 plies, alternating +/- 90 degrees. RCC has an outer layer (several plies) that has been treated to produce SiC to protect the carbon from oxidation at the high re-entry temperatures. The outer layer was not specifically modeled. Instead, each ply was modeled using the smeared laminate properties. Other important RCC parameters are the strength in tension, compression, and shear plus an erosion parameter, "ERODS," that must be empirically determined. If ERODS is too small, the material will fail too early. If ERODS is too large, the material will fail too late and will deform too much. From an early study of foam impacting simply-supported RCC coupons, an ERODS value of 0.1 gave reasonable results and was used in this model. The ERODS, SLIMC, and SLIMT parameters used in Mat58 have remained "fixed" since late 2003 [2]. Since the RCC material properties vary by a considerable degree, six standardized RCC models were constructed: minimum, average, and maximum strength as-fabricated; and minimum, average, and maximum strength flight degraded. In addition, these six different models had to be constructed for each of the different RCC thicknesses used (19 plies, 0.233-in. was the nominal thickness).

Two RCC damage modes of particular concern are front surface SiC coating loss plus internal RCC delamination. Such damage had been noted to produce complete burn-through on test RCC panels that were subjected to arc-jet testing. Also, the LS-DYNA RCC shell model does not directly predict either coating loss or delamination. It was speculated that if delamination occurred early in the 3-point bend test, then the damage parameters that are generated in the Mat58 RCC material model could be correlated with the onset of RCC delamination. If no delamination occurred, then the fallback position was to calibrate the Mat58 damage parameter(s) to first detectable NDE damage for the 3-point bend test, which is a one-dimensional test with simple boundary conditions.

The model discretization is shown in Figure 15 below. The load was applied in equally divided increments over 9 nodes at the center. Simple-support boundary conditions were applied at the positions of the two rollers [3].

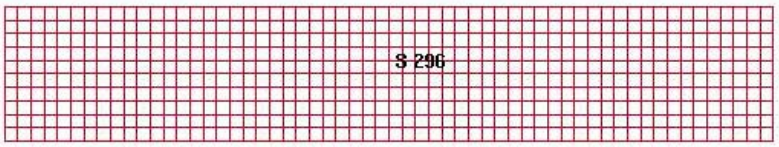

Figure 15. Simple 3-point specimen discretization

Test-Analysis Correlation

Since Mat58 is not implemented in the implicit version of LS-DYNA that one would ordinarily use for a static simulation, a dynamic simulation was performed sufficiently slowly that the kinetic energy was negligible as compared with the strain energy in the RCC flex specimen. It was found that a total load of 145 pounds applied linearly in time over 30 milliseconds gave reasonable results. The damage parameter in the X-direction (the long axis of the coupon) is shown in Figure 16 for each of the 19 layers versus time for shell element 296 located near the center of the specimen. Note that RCC is weaker in tension than in compression. Since 1 and 2 are the principal directions in the local axis system, the damage parameters for the X-direction alternate with each +/- layer. History variable #2 is maximum for layer 1, which is labeled "J" in Figure 16. The history variable (damage parameter) in the X-direction increases dramatically from 0.88 to 0.94 around 0.025 seconds, which is about 120 pounds. This behavior should correspond theoretically to large damage accumulation and perhaps the threshold of NDE detectable damage. The average failure load occurred in the tests at 128.6 pounds, which was well predicted as shown in Figure 17. As noted in the experimental section, the suite of NDE techniques had difficulty in finding either internal damage or the cracking of the SiC. A hint of RCC damage was not detected by ultrasonics in flex-1 until 130 lbs, which corresponded to a damage parameter of 1.0 as shown in Figure 17. However, the model predicted complete failure at 128 pounds. The initial failure for the bend tests was always a tension crack in the lower ply. In the static bend tests, delaminations either did not occur, or if delaminations did occur, they occurred very late in the loading sequence as for the short beam shear test. For dynamic impact tests, internal damage/delamination can be readily detected by NDE such as thermography and ultrasonics. Internal NDE detectable damage for dynamic impacts onto RCC occurs early in the damage sequence (before through cracks and before coating loss). For dynamic tests, the maximum damage parameter for NDE detectable damage ranged from 0.95 to 0.98. The static bend tests were not useful for accurately calibrating the damage parameter to internal NDE detectable damage.

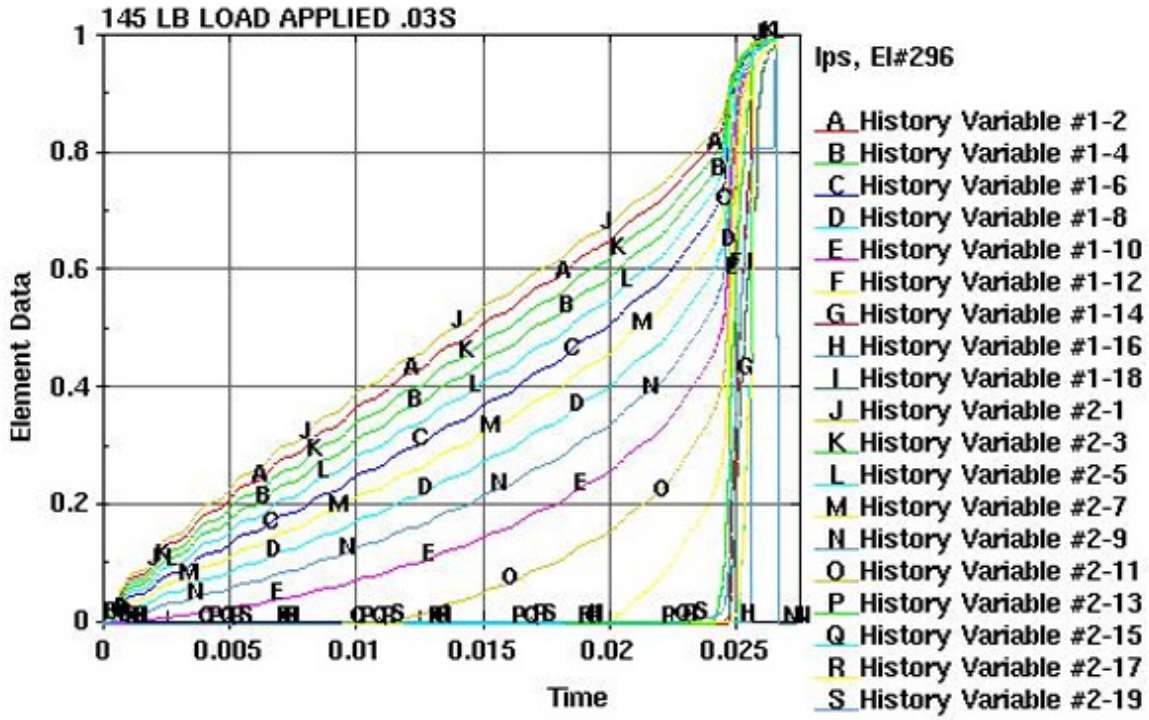

Figure 16. Damage parameter for a center element 296 versus time.

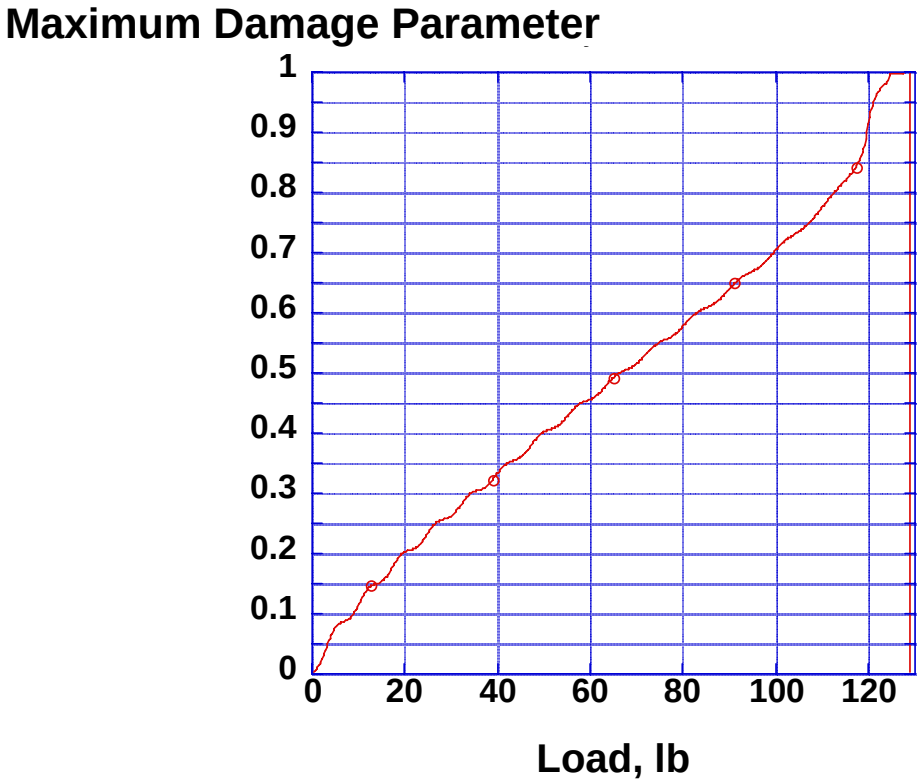

Figure 17. Maximum history variable plotted versus load (bottom ply). Note the steep drop off at approximately 128 pounds indicates complete failure has occurred.

In addition to damage predictions, the maximum center displacement versus time is used in dynamic validation studies. Statically, a comparison of displacement versus load is a good indicator of model validity. Thus, a comparison of experimental load versus displacement (colored curves) with analysis (black) is shown in Figure 18. Note that the analysis used smeared (laminate) RCC properties. Young's modulus in tension is smaller than the modulus in compression for the laminate. Since the initial modulus (E) used in this study is the compression modulus, the analytical displacements at first lag the measured displacements. However, by 0.16-inches of displacement, the analysis, and test data intersect.

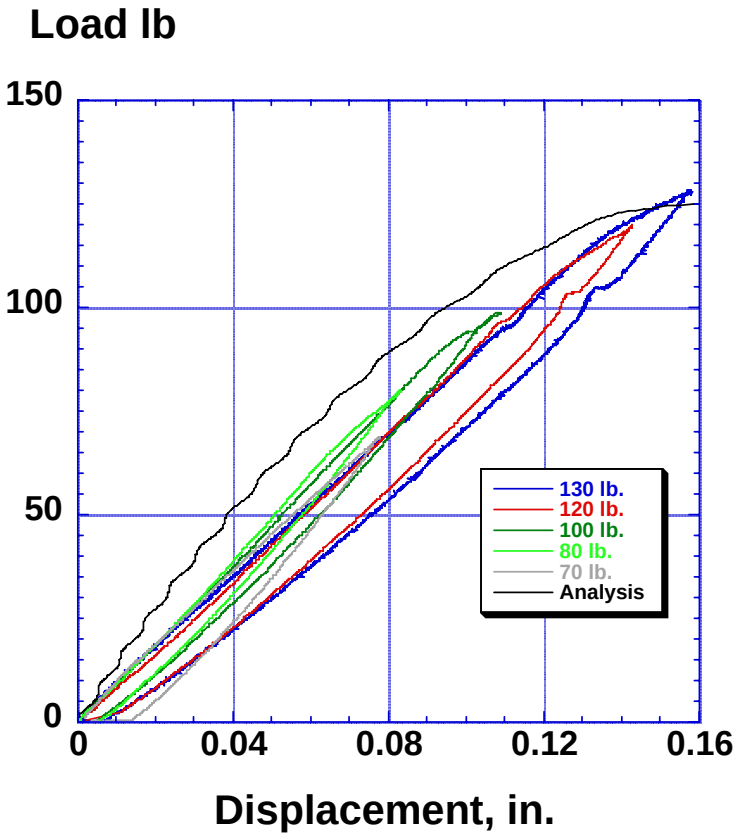

Figure 18. Load versus displacement of test versus analysis.

Concluding remarks

The definition of damage threshold used by the Orbiter Project was changed from a through crack to internally detectable NDE damage plus some outer SiC coating loss. This new definition of damage threshold presented a challenge in modeling the RCC since delamination and coating loss cannot be directly represented using a single shell element. Ballistic tests at NASA GRC of foam and ice onto 6x6-in RCC flat plates showed that internally detectable NDE damage could be correlated with LS-DYNA Mat58 damage parameters. However, ballistic tests are hard to control. To further increase the confidence in the damage parameter correlation, the NESC proposed that a static 3-point bend test be used to further calibrate internal damage with the Mat58 damage parameters.

One must, however, keep in mind that static and dynamic damage and failure mechanisms are often very different. Static tests allow the entire structure to move without inertial loading effects. Thus, the forces are more global and the internal stresses are usually lower and more distributed. Dynamic loads are rapidly applied, produce shock effects with complex stress waves, inertia becomes extremely important, strain-rate effects must be considered, and the stresses are both much higher and localized near the area of contact.

A series of RCC bend or flex specimens, all 1-in. x 5.8-in. and 19 plies thick, were statically loaded in a 3-point bend apparatus. The objectives of these tests were: (1) The failure load and mechanism was to be determined. (2) LS-DYNA models were constructed and the failure load predicted by LS-DYNA was to be compared with the test results. (3) The damage parameter in the LS-DYNA Mat58 RCC material model was to be correlated, if possible, with NDE detectable measured internal damage. Thus, a major objective for the tests was to produce internal damage such as delaminations in the specimen. Unfortunately, no delaminations were produced in the 5.8-in. long three point bend tests. The first failure was always a tensile failure in the bottom layers of the specimen that rapidly lead to complete failure of the specimen.

In this test-analysis correlation, the maximum damage parameter increases dramatically from 0.88 to 0.94 at a load near 120 lbs. This jump is near what is most likely the NDE detectable damage load. Experimentally, failure occurred at an average load of 128.6 lbs (+/- 3.2 lbs). First detectable NDE damage by ultrasonics was for a specimen loaded up to 130 pounds.

In summary, this test showed that LS-DYNA was quite accurate in predicting the failure load, and was good in matching the load versus deflection. However, matching the NDE detectable damage with the maximum damage parameter was not straightforward due to the difficulty in finding cracks and especially internal damage with NDE and the high sensitivity of the damage parameter to the load near failure. One must keep in mind that damage mechanisms in RCC due to impact are not equivalent to damage mechanisms obtained during static loading due to the 3-point bending.

References

1. A. Matzenmiller, A.; Lubliner, I. J.; and R.L. Taylor, R. L.: “A constitutive model for anisotropic damage in fiber-composites.” *Journal of Mechanics and Materials*, Vol. 20, pp. 125-152, 1995.

2. Carney, K.; Melis, M.; Fasanella, E.; Lyle, K; and Gabrys, J.: “Material Modeling of Space Shuttle Leading Edge and External Tank Materials for Use in the Columbia Accident Investigation.” Proceedings of 8th International LS-DYNA User’s Conference, Dearborn, MI, May 2-4, 2004.

3. Fasanella, E. L., Jackson, K. E., Lyle, K. H., Jones, L. E., Hardy, R. C., Spellman, R. L., and Stockwell, A. E., "Dynamic Impact Tolerance of Shuttle RCC Leading Edge Panels Using LS-DYNA." AIAA Paper 2005-3631, July 2005.

REPORT DOCUMENTATION PAGE

Form Approved
OMB No. 0704-0188

1. REPORT DATE *(DD-MM-YYYY)*	2. REPORT TYPE	3. DATES COVERED *(From - To)*
01- 09 - 2006	Technical Memorandum	

4. TITLE AND SUBTITLE

Quasi-Static 3-Point Reinforced Carbon-Carbon Bend Test and Analysis for Shuttle Orbiter Wing Leading Edge Impact Damage Thresholds

5a. CONTRACT NUMBER

5b. GRANT NUMBER

5c. PROGRAM ELEMENT NUMBER

6. AUTHOR(S)

Fasanella, Edwin L.; and Kellas, Sotiris

5d. PROJECT NUMBER

5e. TASK NUMBER

5f. WORK UNIT NUMBER

377816.06.03.03.07

7. PERFORMING ORGANIZATION NAME(S) AND ADDRESS(ES)

NASA Langley Research Center
Hampton, VA 23681-2199

8. PERFORMING ORGANIZATION REPORT NUMBER

L-19275

9. SPONSORING/MONITORING AGENCY NAME(S) AND ADDRESS(ES)

National Aeronautics and Space Administration
Washington, DC 20546-0001

10. SPONSOR/MONITOR'S ACRONYM(S)

NASA

11. SPONSOR/MONITOR'S REPORT NUMBER(S)

NASA/TM-2006-214505

12. DISTRIBUTION/AVAILABILITY STATEMENT

Unclassified - Unlimited
Subject Category 24
Availability: NASA CASI (301) 621-0390

13. SUPPLEMENTARY NOTES

An electronic version can be found at http://ntrs.nasa.gov

14. ABSTRACT

Static 3-point bend tests of Reinforced Carbon-Carbon (RCC) were conducted to failure to provide data for additional validation of an LS-DYNA RCC model suitable for predicting the threshold of impact damage to shuttle orbiter wing leading edges. LS-DYNA predictions correlated well with the average RCC failure load, and were good in matching the load vs. deflection. However, correlating the detectable damage using NDE methods with the cumulative damage parameter in LS-DYNA material model 58 was not readily achievable. The difficulty of finding internal RCC damage with NDE and the high sensitivity of the mat58 damage parameter to the load near failure made the task very challenging. In addition, damage mechanisms for RCC due to dynamic impact of debris such as foam and ice and damage mechanisms due to a static loading were, as expected, not equivalent.

15. SUBJECT TERMS

Carbon-Carbon; Orbiter; Quasi-Static; RCC; Reinforced; Wing

16. SECURITY CLASSIFICATION OF:			17. LIMITATION OF ABSTRACT	18. NUMBER OF PAGES	19a. NAME OF RESPONSIBLE PERSON
a. REPORT	b. ABSTRACT	c. THIS PAGE			STI Help Desk (email: help@sti.nasa.gov)
					19b. TELEPHONE NUMBER *(Include area code)*
U	U	U	UU	25	(301) 621-0390